AD 296 788

MASSACHUSETTS INSTITUTE OF TECHNOLOGY
LINCOLN LABORATORY

MAGNETIC PROPERTIES OF A SINGLE CRYSTAL OF MANGANESE PHOSPHIDE

E. E. HUBER, Jr.

Group 53

TECHNICAL REPORT NO. 280

18 DECEMBER 1962

LEXINGTON MASSACHUSETTS

MAGNETIC PROPERTIES OF A SINGLE CRYSTAL OF MANGANESE PHOSPHIDE*

ABSTRACT

Magnetic measurements were made on a spherical single crystal of high-purity stoichiometric MnP with a vibrating sample magnetometer which was modified to allow precise temperature control and temperature cycling from 4° to 500°K. Anistropy, saturation magnetization, and susceptibility data were obtained over this temperature range.

Evidence is presented which shows that MnP is neither ferrimagnetic nor antiferromagnetic with weak superimposed ferromagnetism, as has been previously supposed. Strong ferromagnetic coupling between spins may be assumed from the fact that the $1/\chi$ vs T curve has strong concave-up curvature above the Curie point.

A magnetic transformation, not previously reported, was observed at 50°K which may be interpreted in terms of temperature-dependent, competing antiferromagnetic-ferromagnetic interactions. Below 50°K, MnP is metamagnetic, i.e., it exhibits an antiferromagnetic-ferromagnetic transition which is a function of applied field and temperature.

* This report is based on a thesis of the same title submitted in partial fulfillment of the requirements for the degree of Doctor of Science in the Department of Metallurgy at the Massachusetts Institute of Technology.

TABLE OF CONTENTS

MAGNETIC PROPERTIES OF A SINGLE CRYSTAL OF MANGANESE PHOSPHIDE

I. INTRODUCTION

The object of this report is an experimental investigation of the magnetic properties of a pure, stoichiometric single crystal of the intermetallic compound MnP in the temperature range 4.2° to 500°K. This material is of interest because of a lack of knowledge concerning its properties, and because the results of the few previous investigations which have been carried out have led to inconsistencies. Previous work has not gone below 77°K, and the investigators have not had the benefit of single crystals for study. One of the main reasons that a single crystal is to be preferred for magnetic measurements is that the saturation moment and spontaneous moment can be determined far more reliably than for a polycrystal, due to the complicating effects of anisotropy in the latter. However, additional benefits are derived from single crystal measurements as becomes apparent in later sections of this report.

Ordinarily a complete magnetic description of a material would require magnetization vs field curves, at all temperatures, for all directions in the crystal. Such a presentation of data would be hopelessly cumbersome and does not shed any light on the fundamental interactions giving rise to the properties concerned. The emphasis in this presentation will be upon those magnetic properties that help to give insight into atomic magnetic interactions.

With this emphasis in mind, it should be stated at the outset that there are two important results of this investigation.

(a) Interactions at high temperatures are ferromagnetic. This eliminates previous speculation that the crystal is ferrimagnetic[1] or contains strongly canted spins.[2] Such speculations were advanced to account for a discrepancy between a higher atomic moment to be inferred from high-temperature, paramagnetic measurements and a lower atomic moment to be inferred from the low-temperature saturation magnetization measments.

(b) MnP has been found to become metamagnetic below 50°K, i.e., it exhibits an antiferromagnetic-ferromagnetic transition that is a function of applied field and temperature. One way of interpreting this phenomenon is in terms of temperature-dependent, competing antiferromagnetic-ferromagnetic interactions.

These conclusions have been arrived at by comparing specific theories of magnetism, such as the Weiss-Heisenberg theory of ferromagnetism or the Néel model of ferrimagnetism, to the results of the magnetic measurements on MnP. Accordingly, a discussion of those theoretical concepts pertinent to interpreting the magnetic data will precede an account of the particular history of research on MnP. The latter discussion is followed by a presentation of results and a discussion. The scope of the theoretical discussion is limited to those concepts and theories

that bear directly on the MnP problem. No attempt is made to establish the fundamental nature of the interactions (such as whether they are direct or indirect) or to establish a specific model of the paths and magnitudes of the interactions.

A. Types of Magnetic Order and Magnetic Measurements

The success of molecular field theory in describing the magnetic behavior of materials make it of paramount importance in classifying and interpreting magnetic data. A measure of the atomic moment and the magnitude of the interatomic couplings is of fundamental importance for this theory of magnetism. Unfortunately, it is difficult to obtain a direct measure of the net coupling between an individual pair of atoms because of the presence of interactions with other neighbors or next near neighbors which may even be competing with the pair interaction in question. The signs and magnitudes of these individual pair interactions can only be inferred, via molecular field theory, from a knowledge of the low-temperature magnetic order, the ordering temperatures, and the character of the high-temperature paramagnetic susceptibilities. Since neutron diffraction experiments can often directly establish the magnetic order, it is natural to classify magnetic materials in terms of their magnetic order rather than in terms of the individual pair interactions that give rise to this order. Accordingly, the types of order pertinent to the MnP problem will be described in what follows, together with a description of typical magnetic properties associated with each type of order, as accounted for by molecular field theory.

MnP is paramagnetic at high temperatures and ferromagnetic at lower temperatures, followed by a type of antiferromagnetism at very low temperatures. The phenomenological theory of ferromagnetism first developed by Weiss[3] and later explained by Heisenberg[4] and others on quantum mechanical grounds goes a long way to explaining, at least qualitatively, the major features of ferromagnetism and paramagnetism. It predicts that the ratio of the magnetization M to the saturation moment at T = 0°K, M_o, should be given by the well-known Brillouin function:

$$\frac{M}{M_o} = \frac{2J+1}{2J} \coth \frac{(2J+1)}{2J} a - \frac{1}{2J} \coth \frac{a}{2J} \qquad (1)$$

where J is the total angular momentum quantum number, $a = [Jg\beta(H + NM_s)/KT]$, g is the gyromagnetic ratio, β the Bohr magneton, and $H + NM_s$ is the total internal field. The quantity NM_s is the Weiss molecular field. When H = 0, the formula yields M_s, the spontaneous magnetization, instead of M. The theory predicts a spontaneous moment that decreases with increasing temperature T up to a critical ordering temperature, the Curie point T_c, above which M_s is zero. Above T_c the susceptibility $\chi = M/H$ should follow a Curie-Weiss Law $\chi = C/(T - \Theta_p)$, which can be obtained from expanding the Brillouin function for high temperatures. These features are shown schematically in Fig. 1(a) by the dashed lines. The inverse susceptibility $1/\chi$ should be linear with temperature above the Curie point; its intercept gives the paramagnetic Curie temperature Θ_p and its slope gives the Curie constant C, from which the effective paramagnetic moment (given atomic multiplet separation $\Delta >> kT$) is obtained by the relation

$$\mu_{eff} = g\sqrt{J(J+1)}\,\beta = \sqrt{8C}\,\beta \quad , \qquad (2)$$

provided C is taken for 1 gram atom of material. The saturation moment at T = 0°K, on the other hand, is $\mu_o = Jg\beta$; it is obtained from the saturation magnetization at T = 0°K, according

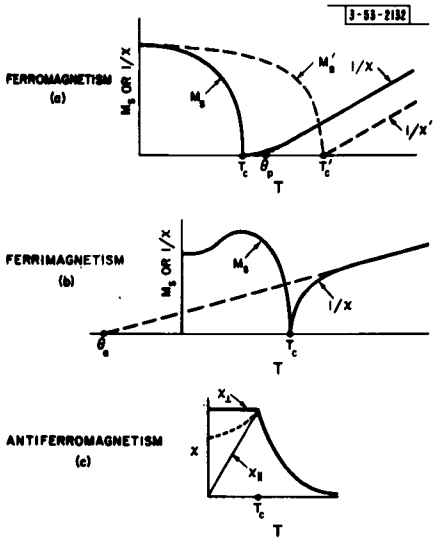

Fig. 1. Typical magnetic properties for different types of magnetic order. (a) Dashed curves refer to the unmodified Weiss-Heisenberg theory; the solid curve refers to more refined calculations as explained in the text. (b) The dashed line is the extrapolation to give the paramagnetic Curie temperature, θ_a. (c) $\chi_\perp$ is the susceptibility perpendicular to the spin axis, $\chi_\parallel$ is parallel to the spin axis, and the dashed line is for a polycrystalline material.

to $\mu_o = M_o A/N_o d$, where M_o is the saturation magnetization at T = 0°K, A is the molecular weight, d is the density, and N_o is Avogadro's number which equals 6.023×10^{23}.

This simple theory gives a fairly good description of ferromagnetism. The ferromagnetic metals Fe, Co, and Ni fit fairly well a Brillouin function for J = 1. Also, agreement between μ_o and μ_{eff} is fair, the latter values being about 15 to 25 percent too high[5]. One consistent disagreement is found in the $1/\chi$ vs T curve which has a concave-upward slope just above T_c, as shown by the heavy line in Fig. 1(a). Refinements[6] of the Weiss-Heisenberg theory, which were made by including the effects of short-range order, have established that $1/\chi$ vs T ought to have this upward curvature. This means that $T_c < \Theta_p$, if predominantly ferromagnetic interactions are present.

The Weiss-Heisenberg theory of ferromagnetism is a model of localized atomic moments obeying Maxwell-Boltzmann statistics. A band-theory approach has been provided by Stoner[5,7] who assumed the magnetism to come from collective (conduction) electrons obeying Fermi-Dirac statistics. He also obtained curves having the essential features of the solid curves in Fig. 1(a) and showed that band theory could account for the experimentally observed curvature in the $1/\chi$ vs T curve. This theory is also able to account for the observed differences in J inferred from μ_o and μ_{eff} in Fe, Co, and Ni.

Just which of the above two approaches best describes a particular material depends on how tightly bound the magnetic electrons are. Obviously, the Stoner treatment works best for the case of loosely bound, almost free electrons. In fact, for very broad bands Stoner's theory reduces to the temperature-independent paramagnetism of Pauli that is characteristic of nonferromagnetic metals. It is not entirely clear whether MnP best fits a narrow-band collective or a localized electron picture; but regardless of which theory applies, the $1/\chi$ vs T curve should be concave-up if the interactions are ferromagnetic. This fact will be used in the discussion of the high-temperature data.

There is a large class of materials whose magnetic properties cannot be satisfactorily explained by either of the above theories, although these materials exhibit an ordering temperature above which they are paramagnetic, and below which they have a spontaneous moment. These materials exhibit ferrimagnetism. Given collinear spins, a ferrimagnet has antiparallel coupling

between two sublattices whose net moments are of unequal magnitude, as shown schematically in Fig. 2(a). A special case of ferrimagnetism, namely antiferromagnetism, occurs when the sublattices have equal moments as shown in Fig. 2(b). If the atomic moments of one sublattice of an antiferromagnet are rotated clockwise through a small angle θ, and those of the other sublattice are rotated counterclockwise, the configuration is no longer collinear and a net ferromagnetic component is superimposed on the antiferromagnetic array. Such "canted-spin" antiferromagnets give rise to "parasitic" ferromagnetism. Since previous speculation has considered MnP to be either a ferrimagnet, or an antiferromagnet with weak superimposed ferromagnetism, it is worth considering some of the pertinent features of these types of magnetism.

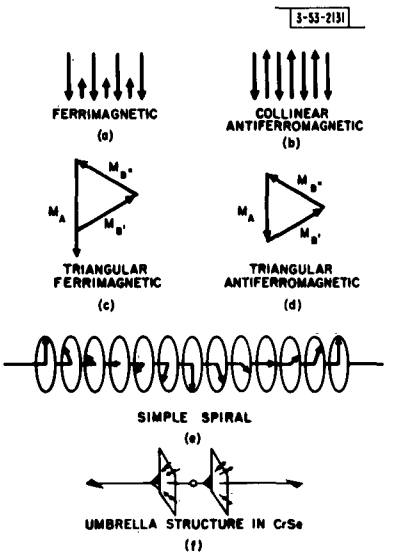

Fig. 2. Types of magnetic order. The arrows signify the directions and magnitudes of the magnetic moments on different atoms.

Néel[8] first successfully extended the Weiss-Heisenberg theory to a two-sublattice system of collinear interacting moments and was able to explain, at least qualitatively, the magnetic data for this type of material. Because two sublattices couple antiparallel, the resulting magnetization is actually the difference between an $M_s(T)$ curve for each sublattice. This has these consequences: (1) μ_o is far below that predicted from μ_{eff} and the assumption of ferromagnetic order. (2) The $M_s(T)$ curves may have unusual, non-Brillouin shapes, even exhibiting maxima or a "compensation" temperature $T_{comp} < T_c$ as the dominant moment shifts from one sublattice to the other with changing temperature. (3) In the paramagnetic region ($T > T_c$) the paramagnetic Curie temperature must be negative, reflecting the antiferromagnetic character of the predominant intersublattice Weiss field. This negative paramagnetic Curie temperature is designated θ_a to distinguish it from θ_p for ferromagnetism. The explicit Néel formulas for the susceptibility are given in Appendix A. It is seen from Appendix A that θ_a is a measure of the average strength of the intersublattice interaction W_{12} and the two-intrasublattice interactions W_{11} and W_{22}. If these latter are ferromagnetic, it is possible to have $\theta_a > 0$; but always $\theta_a < T_c$, which is to be contrasted with $\theta_p > T_c$ for ferromagnetism. Further, the fact that $\theta_a < T_c$ requires that the $1/\chi$ vs T curve be concave-downward between T_c and the high-temperature linear portion, as shown in Fig. 1(b). Finally, the Néel equations predict a high-temperature Curie-Weiss Law from which μ_{eff} can be obtained, and the μ_{eff} is seen to be the

sum of the effective moments on each of the sublattices. These distinctive features have been found experimentally to be characteristic of collinear ferrimagnets.

The magnetic data characteristic of collinear antiferromagnetism is shown schematically in Fig. 1(c). There is a critical ordering temperature T_c at which point the temperature dependence of the susceptibility changes from a Curie-Weiss Law to a more complicated behavior. As for the ferrimagnets, the paramagnetic Curie temperature is $\Theta_a < T_c$, and usually $\Theta_a < 0$. Below T_c a collinear antiferromagnet is characterized by a plane in which an external field $H_\perp$ may be applied perpendicular to the spin axis and all susceptibilities $\chi_\perp = M/H_\perp$ are equal in this plane. The reason for the complete symmetry in this plane is that the anisotropy can be neglected in comparison to the large exchange field which tends to keep the moments antiparallel on the two sublattices. Furthermore, the susceptibility measured with $H_{||}$ applied parallel to the spin axis is smaller than $\chi_\perp$ and is denoted by $\chi_{||} = M/H_{||}$. Theory shows that $\chi_{||}$ should approach zero at T = 0°K (if H is parallel to the spin direction, it exerts no torque on the atomic moments, which are all parallel to this direction at T = 0°K) and that $\chi_\perp$ should be temperature independent to a first approximation and equal to $1/W_{12}$. Figure 1(c) shows these features; the dashed line refers to the susceptibility of a polycrystal.

A further consequence of the two-sublattice model of antiferromagnetism is that if a field applied along the spin axis is large enough, it will cause a "spin flipping" such that there is a discontinuous increase of moment with increasing applied field. The analytic expression for this field at T = 0°K is given by[9]

$$H_c = \sqrt{2KW_{12}} \quad , \tag{3}$$

where K is the magnetic anisotropy constant, as defined in Appendix B. The magnitude of this field is on the order of 10^6 oe for most materials and is greater than the DC field normally available in the laboratory. Although spin-flipping transitions have been observed with pulsed fields,[10] they are only observable in the usually available DC fields (10^4 oe in this investigation) if W_{12} is very small, or $T_c \lesssim 4$°K. This point is stressed, because metamagnetism, which is exhibited by MnP, is due to an antiferromagnetic-ferromagnetic transition that occurs at critical fields that are much smaller than those required for spin flipping.

A modification of the collinear, two-sublattice model of antiferromagnetism occurs when the moments of each sublattice are canted with respect to each other. Such canting is usually extremely small. Moriya[11] has given a mechanism for the canting in terms of anisotropic magnetic interactions. Dzyaloshinsky[12] has shown that canting is a consequence of the crystal symmetry. Therefore, symmetry considerations alone will determine whether the rotation of both sublattices are in the same sense, resulting in antiferromagnetism, or in opposite senses, resulting in weak, superimposed ferromagnetism. However, note that the dominant intersublattice interaction for either ferrimagnetism or parasitic ferromagnetism is antiferromagnetic, so that $\Theta_a < T_c$ and the curvature of the $1/\chi$ vs T curve just above T_c must be concave-down.

Néel's application of the Weiss-Heisenberg theory to collinear ferromagnetism and antiferromagnetism is a reasonably good approximation for materials which are susceptible to a two-sublattice treatment and where the internal-field approximation is valid. An extension[13] of the Néel theory to the case of more than two sublattices (there are six cation sublattices in the spinel structure, for example) has shown the possibility of noncollinear moments that make large angles (to be distinguished from small angles of parasitic ferromagnetism) with each other,

as shown schematically in Fig. 2(c) and (d) for ferrimagnetism and antiferromagnetism, respectively. Moreover, if many competing interactions are present, the assumption of an n sublattice configuration is restrictive and it is important to consider the ground state ordered configuration (within the molecular-field framework) if all the atomic moments in the specimen are allowed to vary with respect to one another – such a solution has not been obtained. However, a many-body approach (generalized Luttinzer-Tisza[14] method) has given a rigorous solution for a large class of compounds.[15,16] Under certain conditions of the relative magnitudes of competing magnetic interactions a spiral array of moments may be stabilized such that all the moments within a plane are parallel but their direction changes by constant increments of angle α_o from one plane to the next. The direction about which this precession rotates (the propagation direction) may take any angle to the plane of spins, but a particularly simple configuration is shown in Fig. 2(e) where the propagation direction is perpendicular to the spin plane. The spiral concept introduces a wide variety of configurations. It can be seen that the spiral concept is a more fundamental concept in magnetism than any of the others mentioned because the simpler triangular and collinear structures can be considered as simple screw structures having particular choices of α_o. Much more complex structures have been observed that are combinations of two or more screw components. For instance, the superposition of one screw component with $\alpha_o = 2\pi/3$ on a collinear antiferromagnetic component ($\alpha_o = \pi$) gives the umbrella structure of Fig. 2(f) recently observed in CrSe by Corliss, et al.[17] This is of particular interest because CrSe is a NiAs structure, and the MnP structure may be considered a distorted NiAs structure.

The rare-earth metals with more than half-filled 4f shells (Tb, Dy, Ho, Er, Tm) have been found to have spiral or sinusoidally varying spin structures, and they all show ferromagnetism at low temperatures and apparent antiferromagnetism (actually metamagnetism) at high temperatures.[18-23] Dysprosium (Dy) is of particular interest to the MnP problem because its metamagnetic properties have been explained by Enz[24] on the basis of a simple spiral model. Behrendt, Legvold, and Spedding[18] have investigated the magnetic properties of Dy and find that in its antiferromagnetic temperature range (85° to 178.5°K) ferromagnetism may be induced by applying a magnetic field surpassing a critical field H_c. Moreover, the value of H_c is small, ranging from 0 oe near the antiferromagnetic-ferromagnetic transition at 85°K to about 10,000 gauss at 160°K. Enz has shown that a spiral is stabilized for ferromagnetic near-neighbor interactions competing with antiferromagnetic next-near-neighbor interactions, provided the next-near-neighbor interactions exceed a critical strength. Furthermore, he has calculated a critical field H_c given by

$$H_c = \frac{1}{8J_2}(J_1 + 4J_2)^2 \quad , \tag{4}$$

where $J_1 > 0$ and $J_2 < 0$ are the exchange constants for near neighbors and next near neighbors, respectively. The condition for the formation of a spiral is given as $|4J_2| > |J_1|$; hence, if J_1 and J_2 vary as functions of temperature, there may be a critical temperature for spiral formation and a critical field for the reestablishment of ferromagnetism. Such a critical field increases from zero with ΔT, where ΔT is the temperature interval from the critical temperature. Moreover, the magnitude of this field can be quite low (in contrast to the spin-flipping field for a collinear antiferromagnet) since the equation involves the difference between two exchange constants, and the difference between two large numbers may be quite small.

The simple spiral configuration of Fig. 2(e), like the collinear antiferromagnet, is characterized by a plane in which all the susceptibilities are equal to the extent that anisotropy within this plane can be neglected. Yoshimori,[25] Kaplan[26] and others have shown that, at T = 0°K, $\chi_{||}$ (H applied perpendicular to the plane of spins or parallel to the propagation vector) should be greater than $\chi_{\perp}$ (H applied in the plane of spins and perpendicular to the propagation vector) if the anisotropy is negligible. They have also shown that $\chi_{\perp}$ does not approach zero at T = 0°K. These results can be anticipated immediately from the geometry. For $\chi_{||} = M/H_{||}$, the field $H_{||}$ is perpendicular to all the atomic spins so that the torque exerted by $H_{||}$ on any moment is a maximum. For $\chi_{\perp} = M/H_{\perp}$, the field $H_{\perp}$ makes a variety of angles with the different atomic moments, so that the torque is never zero, but is always less than maximum. Magnetic anisotropy introduces important modifications into these conclusions if the anisotropy energy is large compared to the difference in exchange energies. The condition would be $K \cong (J_1 + 4J_2)$ in the Enz formulation. These ideas will enter the interpretation of the low-temperature susceptibility data on MnP.

B. Previous Work on MnP

Structural considerations, coupled with inconsistencies in the previous magnetic data have led certain investigators to attempt to explain the magnetization of MnP on the basis of either ferrimagnetism or antiferromagnetism with weak, superimposed ferromagnetism (canted spins). MnP has an orthorhombic, slightly distorted NiAs structure (B31),[27,28] and there is some indirect evidence to indicate that it is an intermetallic compound with a narrow range of composition.[29] The NiAs structure consists of a close-packed hexagonal As sublattice with Ni atoms in the octahedral interstices forming a simple hexagonal sublattice as shown in the exploded view of Fig. 3(a). Figure 3(b) consists of projections parallel and perpendicular to the hexagonal plane. The corresponding orthorhombic cell of MnP has been outlined in heavy black lines in Fig. 3(b), and Fig. 4 is an enlarged view of this projection showing the particular distortions of the MnP structure. Comparison should be made between Fig. 3(b) and Fig. 4. Definition of the orthorhombic axes is ambiguous in the literature. The axis convention a > b > c will be used in this investigation, then the NiAs c axis becomes the MnP b axis, and a NiAs a axis becomes the MnP c axis. The important thing to note is that in MnP the Mn atoms form zig-zag chains along the b axis and the P atoms form zig-zag chains along the a axis. This allows the Mn sublattice to be separated into two sublattices as shown by the labels I and II in Fig. 4. If the Mn atoms of each sublattice are similar, antiferromagnetism is possible and canting would give rise to a superimposed ferromagnetism. If the Mn atoms of the two sublattices are different, ferrimagnetism is possible.

Early magnetic investigations on MnP have not had the benefit of single crystals, nor have the data gone any lower than 77°K. Bates[30] and Whitmore[31] did some of the first magnetic studies and found an effective paramagnetic moment $\mu_{eff} = 3.69$ Bohr magnetons and a paramagnetic Curie point of $\Theta_p = 315$°K. However, their material must not have been pure MnP since it lost its ferromagnetic properties below 303°K in disagreement with the results of later investigators and the results of this investigation.

Guillaud,[32] in a later study than Bates', has measured the saturation moment of polycrystalline MnP down to 77°K and found an extrapolated spontaneous moment at T = 0°K of μ_o = 1.2 Bohr magnetons. He pointed out that the spontaneous moment is low compared to Bates'

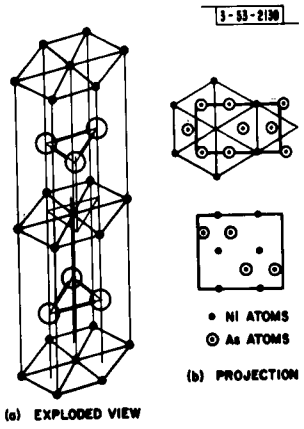

Fig. 3. The NiAs structure. (a) Exploded view. (b) Top figure is a projection on the basal plane. Bottom figure is a projection parallel to an a axis. Heavy lines indicate the corresponding MnP projection in Fig. 4.

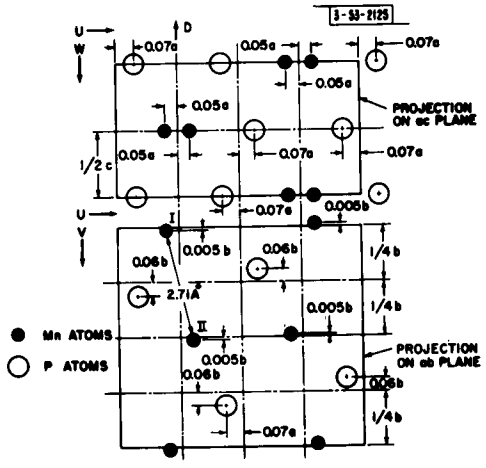

Fig. 4. Projections of the MnP structure. U, V, and W correspond to distances measured along the a, b, and c axes, respectively. The corresponding NiAs projections are shown in Fig. 3(b).

paramagnetic moment and compared to the spin-only value of Mn^{3+} (4 Bohr magnetons). He noted that the structure permits a two-sublattice model of magnetic interactions and therefore speculated that the low moment was due to ferrimagnetism.[33] (He speculated that the two types of Mn atoms carried the electron configuration $3d^5 4S^2$ and $3d^7$.)

Krasovskii and Fakidov[2,34] have performed magnetic and caloric studies on polycrystalline MnP near the Curie temperature. Their measurements of the temperature dependence of the spontaneous magnetization gave the result $(Ms/Mo)^2 = \xi\ (1 - T/T_c)$ with $\xi = 3.4$, where M_s is the spontaneous magnetization at the temperature T, M_o is the saturation magnetization at $T = 0°K$, and T_c is the Curie temperature. They cited theoretical work of Vlasov and Vonsovskii[35] which claims that $\xi > 3$ for metallic, ferromagnetic substances and $\xi < 3$ for ferrimagnetic substances. On this basis, they conclude that MnP behaves somewhat more like a ferromagnet than a ferrimagnet. Therefore, they rejected Guillaud's hypothesis of ferrimagnetism and explained the reduced moment on the basis of the canted spin model mentioned in the preceding section. To account for the observed moment they calculated an angle of 165° between the spins. Note that the canted spin configuration is essentially an antiferromagnetic model.

To summarize, the existing knowledge of the magnetic properties of MnP is not only scanty, it also contains inconsistencies. The low μ_o, and discrepancies between μ_{eff} and μ_o, have

suggested a magnetic order that is either ferrimagnetic or has strongly canted spins. Both models contain antiferromagnetic interactions, which is inconsistent with the high positive value of Θ_p attained from the paramagnetic data of Bates. A value of $\xi > 3$ is probably also inconsistent with the canted spin model of Fakidov and Krasovskii since parasitic ferromagnetism consists of a small ferromagnetic component superimposed on a large antiferromagnetic component.

The availability of a high-purity stoichiometric MnP crystal, coupled with the lack of much previous work on this material, permitted a reinvestigation of the problem. Magnetic investigations on a single crystal are much to be preferred over polycrystalline material for several reasons. First, the complicating effects of high anisotropy make it difficult to determine the saturation, or spontaneous moment. With a single crystal, saturation in an easy direction can be achieved easily at low temperatures. Also, the spontaneous moment can be determined unambiguously near the Curie point, as explained in Sec. II-C. Secondly, the measurement of anisotropy is in itself desirable. Anisotropy serves as an indicator of crystal symmetry, and therefore of possible changes in crystal symmetry. In this investigation, anisotropy plays an important role at low temperatures. A new, low-temperature transformation from ferromagnetism to antiferromagnetism was observed, and it was possible to use anisotropy measurements to check whether the "transformation" could alternatively be explained by a spin-axis jump out of the high-temperature equilibrium position to some new equilibrium position as the temperature is lowered or as the field is increased.

II. EXPERIMENTAL TECHNIQUES

A. Vibrating Sample Magnetometer

A vibrating sample magnetometer of the type first developed by Foner[36] was constructed for this investigation. The advantages of this technique over previous methods lie in the speed with which measurements can be made and the ease with which all the crystallographic directions in a fixed plane can be studied. Several modifications of the Foner technique were necessitated by the particular nature of the MnP problem.

A block diagram showing the basic principle of operation is shown in Fig. 5. A magnetic sample is vibrated by the drive rod at 34 cps which is attached to a loudspeaker driver and driven by an amplitude- and frequency-controlled driver. Voltages from the magnetic sample

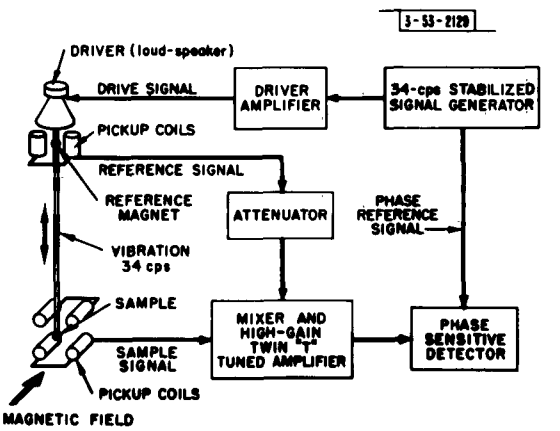

Fig. 5. Magnetometer electronics.

and from the magnetic reference material are simultaneously induced in separate sets of pickup coils. The reference signal is attenuated and bucked against the sample signal in the first stage of a high-gain, twin "T" tuned amplifier, and the output of this amplifier is further amplified and converted to a DC signal by a phase-sensitive detector which is phased relative to the original driver signal. The over-all gain of the amplifier is around 10^9 with 10^{-9} volts detectable, but the presence of vibrational pickup makes some of this gain unusable. The measurement of the magnetization of a sample consists merely of adjusting the reference signal against the sample signal to produce a null and comparing the magnitude of the signal required against the magnitude from a nickel standard.

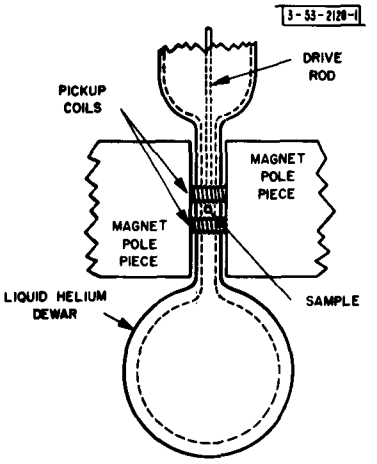

Fig. 6. Temperature control.

One of the modifications of the Foner technique developed in this investigation was in the method of temperature control and temperature measurement. Ordinarily a dewar, such as the one shown in Fig. 6 is used to achieve low temperatures, and measurements are made as the sample warms up continuously in the vapor from the evaporating liquid helium or liquid nitrogen. It was deemed desirable to study the magnetization processes at a fixed temperature, and so this technique was changed to permit stable temperature control to within ±0.04° at high ($T > 200°K$) temperatures, but becoming ±0.2° at low (4.2°K) temperatures, by placing heaters on the sample holder and in the liquid bath. Heat from the sample heater could be balanced against increased cold vapor evolution caused by the heater in the liquid bath. The whole setup was automatically controlled by amplifying the thermocouple voltage from the sample thermometer with a Keithley millimicrovoltmeter (Keithley Instruments, Cleveland, Ohio) and subtracting the output from a preset voltage. The resulting error signal was fed to one or the other of the heaters. A further change was to place a thermocouple directly in contact with the sample instead of just in proximity. This necessitated calibrating a gold-cobalt alloy vs copper thermocouple as it was found that a copper-constantan thermocouple has a measurable magnetic moment. The gold-cobalt alloy has no detectable moment. The thermocouple was calibrated against premium grade copper-constantan wire from the Thermo-Electric Company (Saddle Brook, New Jersey), using their reference tables, which are based on measurements published by the National Bureau of Standards. The absolute accuracy is probably better than ±1°K but the Curie point accuracy in this report is ±0.2°K due to a separate calibration.

Another innovation on the Foner technique consisted of using sample pickup coils parallel to the field direction instead of perpendicular. This was motivated by the need to get as high a field as possible at the sample because of the high anisotropy of MnP. The normal Foner arrangement utilizes a space between the dewar and pole pieces for the pickup coils, and gaps of $2\frac{1}{2}$ to 3 inches are necessary. The parallel arrangement, shown in Figs. 5 and 6 allows the gap to be reduced to 1 inch and a field of 11,000 gauss is possible with only a 4-inch Varian magnet (Varian Associates, Palo Alto, California). With this arrangement a slight slope was observed in the M vs H curve, which is due to some of the magnetic flux from the sample being trapped in the pole pieces instead of going through the pickup coils (a magnetic charge "image" effect). This effect was small and was not deemed objectionable to the particular studies in this investigation. However, another complication with this coil arrangement arose from the increased sensitivity of the pickup coils to mechanical vibrations of the driver and to line voltage transients getting through the stabilized power supply of the magnet. This effect was reduced in seriousness by proper vibration damping of the driver and by designing a filter for the transients in the power supply. Nevertheless, the over-all sensitivity of the instrument is limited by these effects to detectability of a magnetic moment of about 3×10^{-4} emu, which corresponds to a difference in susceptibility of $\Delta\chi = 3 \times 10^{-8}$ for a one-gram sample in a field of 10,000 gauss. This sensitivity is sufficient to permit measurements on most paramagnetic materials with good accuracy for a one-gram sample. The small sample size in this investigation (about 80 mg) caused a 20 percent error in the determination of μ_{eff}.

B. Sample Preparation

The MnP crystal was grown by Dana Ridgley of Lincoln Laboratory in an evacuated quartz tube having two heat zones. Spectroscopically pure Mn pieces were located in one zone and heated at 1150°C for 90 hrs followed by a slow cool. A phosphorus vapor atmosphere was generated by phosphorus placed in the other zone, the temperature of this zone being increased gradually from 400° to 500°C. The phosphorus pressure could thus be low and controlled, whereas the manganese could react at a temperature high enough to allow good mixing. The resulting melt had one irregularly shaped crystal at the surface which was cut into two fragments: one for measurement and the other for analysis. Analysis for Mn showed 50 atomic percent within the error of analysis (±0.3 percent). Spectroscopic analysis showed only 10- to 100-ppm Mg, 10-ppm Si, 1-ppm Fe, and 10-ppm Pb.

The portion of the crystal for measurement was ground into a 0.118-inch-diameter sphere by glass ball milling, and the principal crystallographic directions were located by Laué photographs. The particular crystal axes were discerned by orientation on a diffractometer. Replicas of some of the spots from the Laué photographs are shown in Fig. 7 to aid in further investigations. Sample orientation was facilitated by use of the magnetic easy axis (c axis) to align the sphere on a magnetic pole piece as a start in the orientation process.

During the measurements, the sample was subject to such large magnetic torques and extreme thermal shocks that it was necessary to take elaborate precautions in cementing the sample to its holder. Two cements were needed simultaneously. A silicone rubber cement had good holding qualities at low temperatures and a modified epoxy resin[37] was needed to give rigidity at high temperatures. Completely spurious results were obtained when one or the other of these cements failed to hold. In fact, an anomalous magnetic anneal effect was "observed"

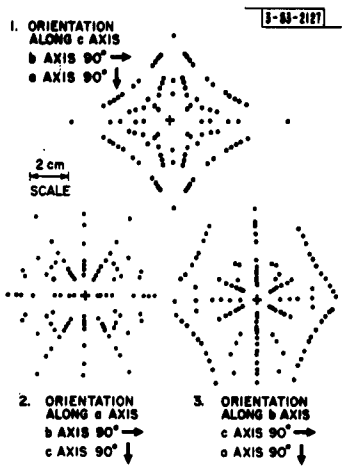

Fig. 7. Laué figures of MnP. These are tracings from the original photographs. Not all the spots have been recorded and so there is some asymmetry. The arrows refer to the directions of the axes in each figure.

for some time until it was discovered that the epoxy cement had cracked, leaving only the rubber cement to hold the sample.

C. Measurement Techniques

Two of the quantities measured in this investigation, the spontaneous moment, and the anisotropy, call for special comment since there are a variety of techniques available for measurement.

The principal problem to be overcome in finding the temperature dependence of the spontaneous moment is the strong curvature of the M vs H curves in the region of the Curie point (see also Sec. III-B). The classic work of Weiss and Forrer[38] on nickel attacked the problem by converting the magnetic data into H vs T curves at constant M. The Weiss[39] theory of ferromagnetism shows that these curves should be straight lines, and Weiss and Forrer extrapolated the linear portions of their H vs T curves back to the H = 0 axis in order to find their values of M_s at a given T. This method, then, is basically a high-field extrapolation method, which relies on how closely the material obeys the Weiss theory.

The method followed in this report is one which has been developed by Smith.[40] He pointed out that the value of M at which the M vs H curve (measured in the easy direction) breaks away from its demagnetizing slope is exactly M_s. If one measures M vs H in the easy direction of a spherical single crystal having few imperfections, one does not obtain a classic rectangular hysteresis loop. Instead, the hysteresis portion of the curve is shrunk almost to zero since the coercive force is often < 1 oe for a good single crystal. Also, the initial portion of the M vs H curve has a slope given by the requirement that the internal field H_i be approximately zero until saturation ($M = M_s$) is reached. Since $H_i = H_e - NM$, this results in $H_e = NM$, where N is the demagnetizing factor of the ellipsoid in the direction of measurement, M is the net magnetization, and H_e is the external field. The slope of the initial (where $M \leqslant M_s$) portion of the M vs H curve, therefore, is 1/N. If $M \geqslant M_s$, it is no longer possible for changes in M to compensate H_i to give $H_i = 0$, and there is an abrupt change in the M vs H curve. The M vs H curves for different temperatures all start out with an initial slope of 1/N, but the breakaway point from this slope, which gives $M_s = H_e/N$, occurs at different critical values of the external field H_e.

Anisotropy is measured in a variety of ways, one of the best being to use the torque magnetometer.[39] However, Néel, et al.,[41] have shown that magnetization curves measured in different directions on a good spherical crystal can be fitted to a simple theoretical expression,

provided the anisotropy is uniaxial. Their expressions, discussed in Appendix B, show that there is a low-field, multidomain region where one set of equations apply and a high-field, single domain region where another set of equations apply. Both of these sets of equations involve the anisotropy, and therefore provide independent ways of measuring the anisotropy. The low-field equations actually provide two methods of measuring the anisotropy and so there are three different methods that have been used in this investigation. All three methods were used for the bc plane at 77°K. The rest of the measurements of anisotropy were made by measurement of the slope of the M vs H curves in the intermediate and hard directions (b and a directions) respectively as outlined in Appendix B. The field necessary to achieve saturation in the a direction of the crystals was prohibitively large (60,000 oe) so that only the low-field set of equations could be used in the (010) plane.

III. RESULTS

Consistent with the approach outlined in the introduction, the results of this investigation will be grouped in three categories. The first group concerns data from the "high" temperature region from 500°K (upper limit of apparatus) down to just above 50°K. In this region MnP goes from paramagnetic to ferromagnetic and the data are pertinent to the previous speculations of ferrimagnetism or weak antiferromagnetism. The second grouping of data is from the low-temperature region, 4.2° to just above 50°K. In this region MnP goes from ferromagnetic to antiferromagnetic with decreasing temperature and the data suggest the hypothesis of competing interactions. The third grouping is a presentation of anisotropy measurements in the ferromagnetic region which shed light on the previous data.

A. High-Temperature Results

The paramagnetic susceptibility of MnP has been measured as a function of temperature and is shown in Fig. 8, where χ_a, χ_b, and χ_c refer to susceptibilities along the a, b, and c axes, respectively, using the axis convention a > b > c. No attempt was made to measure χ_a and χ_b any higher than shown since their magnitudes converged toward χ_c at higher temperatures. No correction has been made for the demagnetizing field in this plot, but the difference between any two values of $1/\chi$ is not sensitive to this effect, as is shown in Appendix B.

From the Weiss theory of ferromagnetism above the Curie point the data of Fig. 8 fit the expression $\chi_g = (C_g/T - \Theta_p)$ with $C_g = 1.23\ 10^{-2}$, where χ_g refers to the susceptibility in emu per gram and $\Theta_p = 39° \pm 1°C = 312° \pm 1°K$. Conversion to C_A and χ_A (susceptibility per gram atom) and use of the expression[42] $\mu_{eff} = \sqrt{8C_A\beta}$ for the effective paramagnetic moment, gives

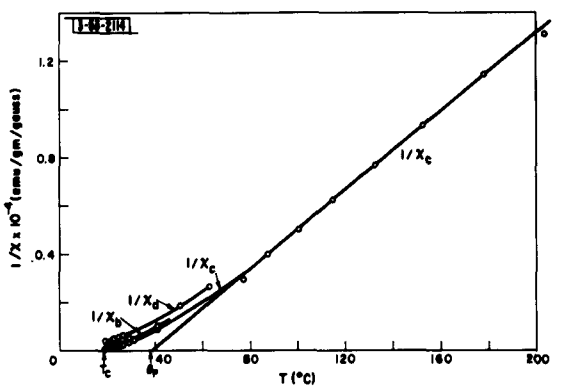

Fig. 8. $1/\chi$ vs T along the a, b, and c axes.

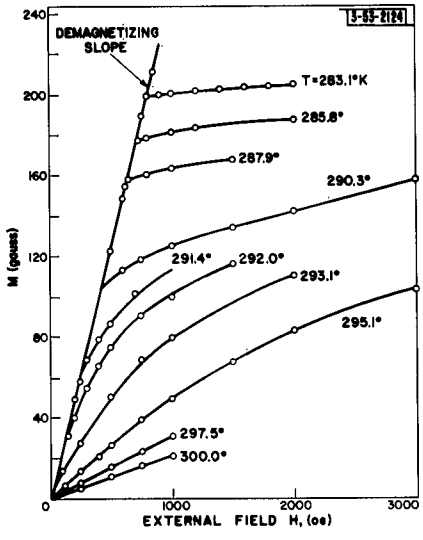

Fig. 9. M vs H along the c axis near the Curie point.

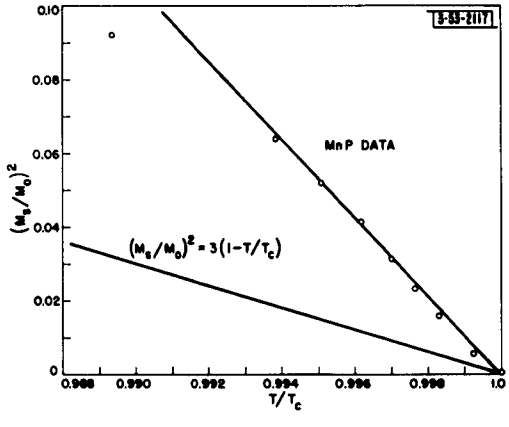

Fig. 10. $(M_s/M_o)^2$ vs (T/T_c) near the Curie point. The point at $(M_s/M_o)^2 \cong 0.092$ shows the beginning of the deviation from linearity.

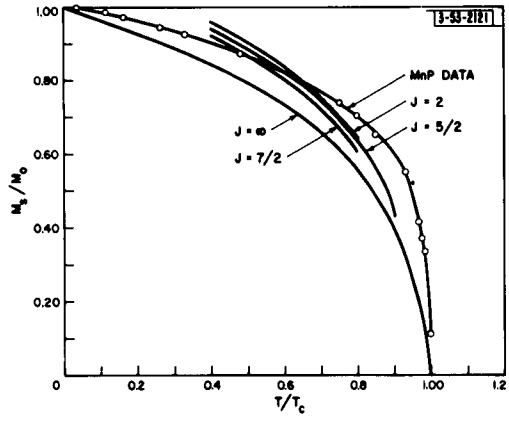

Fig. 11. (M_s/M_o) vs (T/T_c). Comparison of MnP data with Brillouin curves.

TABLE I

VALUES OF $(1/\chi_a - 1/\chi_c)$ ABOVE THE CURIE POINT

$(1/\chi_a - 1/\chi_c)$	Percent of Approximate Error in $(1/\chi_a - 1/\chi_c)$	T°K	$T - T_c$ (deg)	χ_a/χ_b
75	5	289.9	−1.6	16.3
77	6	292.4	+0.9	10.8
76	8	294.8	3.3	4.4
86	8	297.2	5.7	3.34
88	10	299.7	8.2	2.65
91	15	304.4	12.9	2.18
84	45	323.9	32.4	1.26

μ_{eff} = 2.9 Bohr magnetons. The accuracy of this number is only about ±20 percent, due to the small size of the signal compared to the vibrational pickup noise.

It was also found that the difference $(1/\chi_a) - (1/\chi_c)$ is almost constant to within experimental error over a considerable range above the Curie point. Table I shows these values. It can be seen from the table that $(1/\chi_a - 1/\chi_c)$ is approximately constant even though the ratio χ_a/χ_c has changed by over a factor of ten and the temperature to 32.4° above the Curie point. The large error in $(1/\chi_a - 1/\chi_c)$ at higher temperatures is due to taking the difference between two numbers that become increasingly larger.

Figure 9 shows some of the magnetization curves near the Curie point. The method of Smith,[40] previously described, is applicable to finding the temperature dependence of the spontaneous moment $M_s(T)$ since all the magnetization curves for $T < T_c$ have the same initial slope equal to 1/N within the experimental accuracy of ±2 percent where N is the demagnetizing factor for a sphere. Figure 9 is not the actual data used for the Curie point determination. Another measurement of $M_s(T)$ together with a special calibration of T determined the ferromagnetic Curie point ($M_s = 0$) to be $T_c = 291.5 \pm 0.2$°K. Figure 10 is a plot of $(M_s/M_o)^2$ vs (T/T_c) where M_o is the spontaneous moment at T = 0°K and T_c is the ferromagnetic Curie point. It shows that near the Curie point $(M_s/M_o)^2 = \xi(1 - T/T_c)$ with $\xi = 10.8$.

Values of (M_s/M_o) are plotted in Fig. 11 vs (T/T_c) in comparison with portions of Brillouin curves for different values of J. It is seen that no Brillouin curve can fit the observed data, but it is also noted that (M_s/M_o) is a smooth, monotonically decreasing function of (T/T_c). Extrapolation of $M_s(T)$ from T = 4.2°K to T = 0°K gives $4\pi M_o = 6000$ gauss, or $\mu_o = 1.29 \pm 0.04$ Bohr magnetons. (In high fields MnP is ferromagnetic at all temperatures.)

B. Low-Temperature Results

The ferromagnetic data is typified by the M vs H curves shown in Figs. 12 and 13 for different directions in the bc and ac planes, respectively. It is noted that the crystal axes have a magnetic "hardness" of the same relativity as their respective lengths: c is easy, b intermediate, and a hard; and c < b < a. Moreover, this relative hardness is preserved throughout

the entire ferromagnetic and paramagnetic regions. The possibility of other axes becoming easier than the c axis at lower temperatures, resulting in a metastable "easy" axis, was checked by cycling the crystal from above room temperature to the liquid helium range of temperatures in the presence of an applied field. No temperature or magnetic hysteresis effects were noticeable anywhere in the entire temperature range.

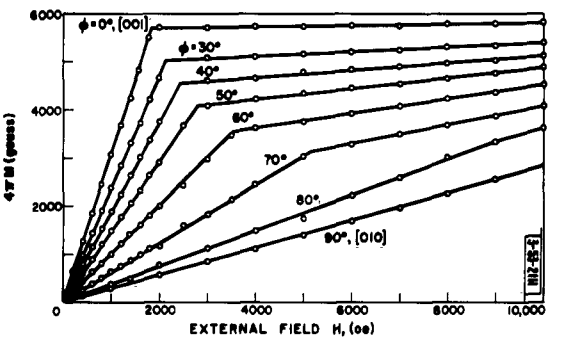

Fig. 12. Magnetization curves at 77°K in the bc plane. ϕ is the angle between H and the c axis and is 0° for the [001] direction and 90° for the [010] direction.

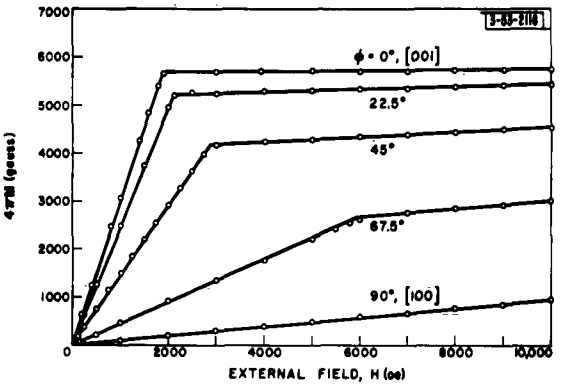

Fig. 13. Magnetization curves at 77°K in the ac plane. ϕ is the angle between H and the c axis and is 0° along the [001] direction and 90° along the [100] direction.

Curves very similar to the ones in Figs. 12 and 13 were obtained at other temperatures between 50° and 291.5°K with modifications coming in three ways: (1) The saturation magnetization dropped with increasing T as discussed in Sec. III-A. (2) A strong curvature developed in M(H) near the Curie point. (3) The slope of M vs H curves measured at angles to the c axis became larger as $T \rightarrow T_c$. The latter effect is due to the temperature dependence of anisotropy and is discussed in Sec. III-C.

At 50°K an abrupt change occurs in the low-field properties of MnP. The consistent trend of properties mentioned above is broken and all of the magnetization curves begin to shift to the right along the H axis and a small initial susceptibility is observed. The start of this process is shown in Figs. 14 and 15 for the bc and ac planes at 47.5°K. The shift has become quite large, by contrast, at 7.3°K as in Figs. 16 and 17 for the bc and ac planes, respectively.

There are three important features brought out by these data:

(1) At 50°K there is an abrupt decrease in the initial susceptibility in the c and b directions of the crystal. This is further shown by Fig. 18, which is a plot of χ_a, χ_b, and χ_c in the low-temperature region. It is seen that χ_a stays relatively constant. The ratio $\chi_a/\chi_c \rightarrow 1$ as $T \rightarrow 0°K$ and within experimental accuracy all susceptibilities in the ac plane were equal at 4.2°K. The ratio $\chi_c/\chi_b = 1.65 \pm 0.05$ at that temperature.

(2) There is a critical field H_c for the c axis at which ferromagnetism is restored. It varies from 0 oe at T = 50°K to almost 2500 oe at 4°K. This interpretation is based on the fact that M vs H changes abruptly at H_c, and thereafter follows a straight line exactly parallel to the demagnetizing slope until saturation is reached. There is no anomaly in the saturation moment on passing through 50°K, as can be seen from Fig. 11.

(3) There is also a critical field effect for the b axis of the crystal (and therefore for all directions in the bc plane), as can be seen from Fig. 16. At high enough field strengths all the curves of Fig. 16 show an abrupt increase in magnetization as the field is increased. Although the

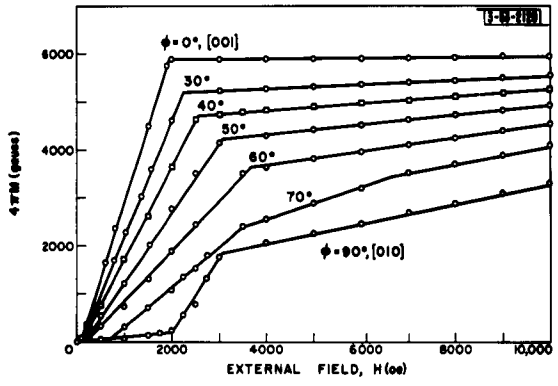

Fig. 14. Magnetization curves at 47.5°K in the bc plane. ϕ is the angle between H and the [001] direction and is 90° for H along the [010] direction.

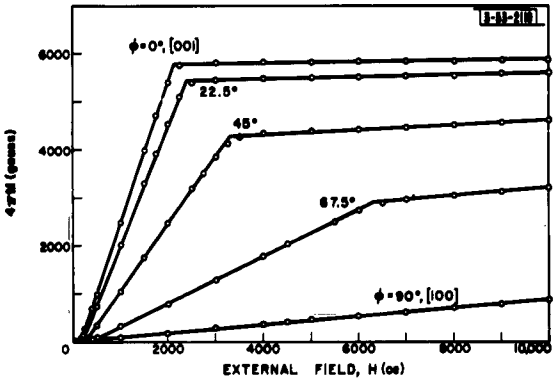

Fig. 15. Magnetization curves at 47.5°K in the ac plane. ϕ is the angle between H and the [001] direction and is 90° when H is along the [100] direction.

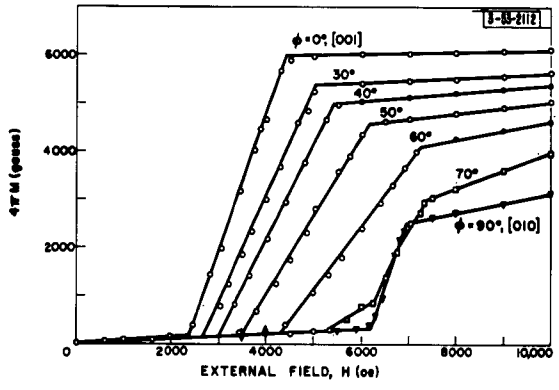

Fig. 16. Magnetization curves at 7.3°K in the bc plane. ϕ is the angle between H and the [001] direction and is 90° when H is along the [010] direction.

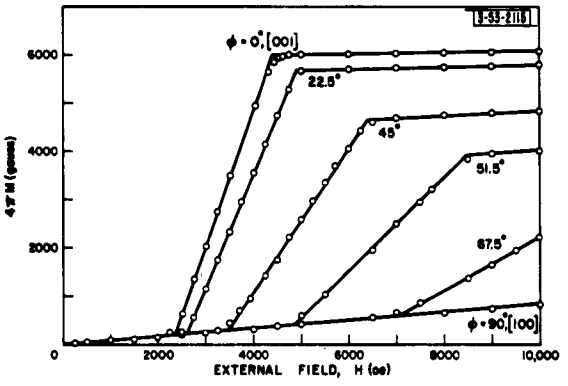

Fig. 17. Magnetization curves at 7.3°K in the ac plane. ϕ is the angle between H and the [001] direction and is 90° when H is along the [100] direction.

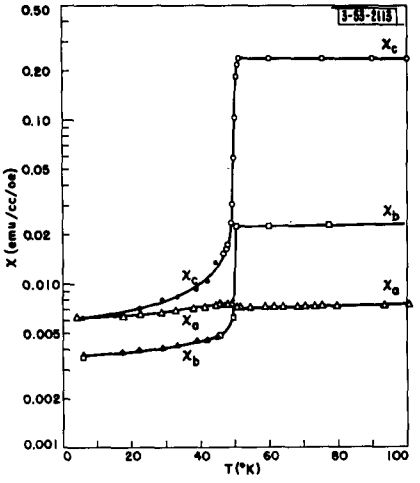

Fig. 18. Initial susceptibility vs temperature along the a, b, and c axes. χ_c is not infinite above 50°K because these are effective susceptibilities, $\chi = M/H_e$, and no correction has been made for the demagnetizing field.

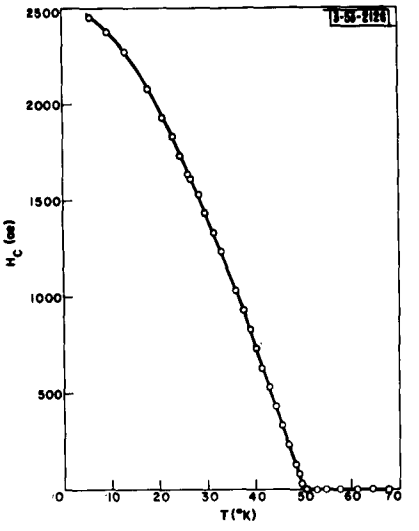

Fig. 19. Critical field for the c axis vs temperature.

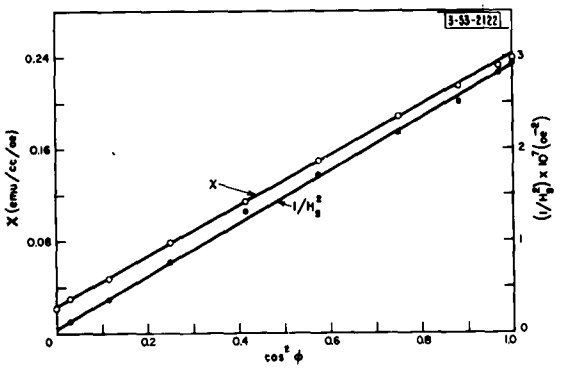

Fig. 20. χ and $(1/H_s)^2$ vs $\cos^2\phi$. Test of the Néel model.

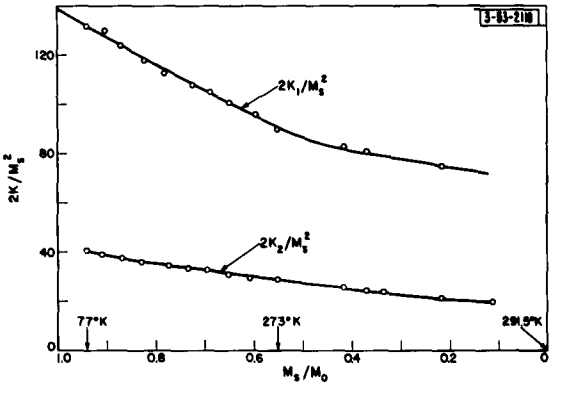

Fig. 21. $2K_1/M_s^2$ and $2K_2/M_s^2$ vs M_s/M_o.

abruptly rising portion of the curve along the b axis in Fig. 16 indicates a critical field, the slope of the step is not equal to (1/N), so that it is not possible to make a straightforward correction for the demagnetizing factor, as in the case of the c axis. The temperature dependence of H_c is shown in Fig. 19.

The interpretation of these data is that the material has become metamagnetic, i.e., it exhibits an antiferromagnetic-ferromagnetic transformation which is a function of the direction and magnitude of the applied field and of the temperature. Additional measurements were made that show that the transition can take place at a temperature higher than 50°K if a strong field is applied along the b axis.

C. Anisotropy Measurements

The shape of the magnetization curves in the bc plane can be described accurately by the Néel theory[41] for the magnetization process in a spherical single crystal having uniaxial anisotropy. The Néel theory predicts that the effective initial susceptibility χ will be proportional to $\cos^2\varphi$ where φ is the angle between the easy (c) axis and the direction of applied field. It also predicts that there is a critical field H_s marking the change from magnetization by domain wall motion to magnetization by rotation and it shows that $(1/H_s^2) \propto \cos^2\varphi$. These relationships are plotted in Fig. 20, where the values for H_s have been determined from the abrupt change in slope in the magnetization curves of Fig. 12. It can be seen in Fig. 20 that the Néel model adequately describes the data.

It is shown in Appendix B how the Néel model can give three different ways of measuring the anisotropy constant. The agreement between three methods of measuring the anisotropy was within experimental error.

The general form for the anisotropy energy of an orthorhombic crystal is given by $E = K_1'\alpha_1^2 + K_2'\alpha_2^2 + K_3'\alpha_3^2$ where higher-order terms in the α's have not been included and where the α's are the direction cosines relative to the crystallographic axes. The trigonometric relationship $\alpha_1^2 + \alpha_2^2 + \alpha_3^2 = 1$ can be used to eliminate a term in α_3, giving $E = K_1\alpha_1^2 + K_2\alpha_2^2 +$ constant. The constant term can be neglected since the derivative of E is used.

Using the axis convention a > b > c, and measurement of α_1 and α_2 relative to the a and b axes, respectively, it was found by the methods of Appendix B that $K_2 = (4.1 \pm 0.4)10^6$ ergs/cc and $K_1 = (1.4 \pm 0.3)10^7$ ergs/cc at 77°K. The latter measurement is based only on the a axis susceptibility since fields sufficient to saturate the material in this direction could not be realized.

The temperature dependences of K_1 and K_2 were measured by the susceptibilities in the a and b direction, respectively, as described in Appendix B and the data are presented in Fig. 21, in terms of the normalized quantities $(2K_1/M_s^2)$ and $(2K_2/M_s^2)$ vs (M_s/M_o) for the sake of comparison with theory. Note that both $(2K_1/M_s^2)$ and $(2K_2/M_s^2)$ do not tend to zero at the Curie point, where $M_s = 0$. This is consistent with Table I, which shows the values of $(1/\chi_a - 1/\chi_c)$ in the paramagnetic state, as is discussed in Sec. IV-C. It is shown there, and in Appendix B and Appendix C, that an effective paramagnetic anisotropy constant K_p (or K_{p1} and K_{p2} corresponding to K_1 and K_2, respectively) can be defined so that $(1/\chi_a - 1/\chi_c) = 2K_{p1}/M_s^2$. The constant value of $(1/\chi_a - 1/\chi_c) \sim 80$ above the Curie point appears to be an asymptote of $2K_1/M_s^2$ of Fig. 21.

IV. DISCUSSION OF RESULTS

A. High-Temperature Data

The salient feature of the high-temperature results is that MnP has strong ferromagnetic interactions. This can be assumed from two facts: (1) The curvature of the $1/\chi$ vs T curve is concave-up near the Curie point. (2) The paramagnetic Curie temperature is relatively high and $\Theta_p > T_c$. The molecular field theory predicts concave-down behavior for a ferrimagnet and a low ($\Theta_a < T_c$) or negative Curie temperature as explained in the introduction. Since the exchange energy of a spin in the Weiss field is on the order of the thermal energy of a spin at the Curie or Néel temperature, the exchange field can be found approximately by equating the two energies.[43] This gives an exchange field H_{ex} of about $+4 \times 10^6$ oe for MnP, which is of the same order of magnitude as in other ferromagnets such as Fe, Co, and Ni. This value ought to be much lower or even negative if strong antiferromagnetic interactions are present, as in a ferrimagnet or in an antiferromagnet with superimposed parasitic ferromagnetism. The value of the Curie or Néel temperature extrapolated from the $1/\chi$ vs T curve is a measure of the average value of the strength of the interactions (see Appendix A) and a change in sign occurs from negative to positive when antiferromagnetic exchange dominates ferromagnetic exchange.

From these considerations it can be concluded that MnP does not fit either a ferrimagnetic model as Guillaud[1] has proposed or a model of antiferromagnetism with weak superimposed ferromagnetism as Krasovskii and Fakidov[2] have suggested. Further support for this comes from measurement of the temperature dependence of the spontaneous moment $M_s(T)$. Fakidov and Krasovskii[34] have found that their polycrystalline MnP data for the spontaneous moment obeyed the relationship $(M_s/M_o)^2 = \xi\,[1 - (T/T_c)]$ where M_o is the spontaneous moment at $T = 0°K$ and $\xi = 3.4$. They cite a work of Vlasov and Vonsovskii[44] who claim, on the basis of an "s-d" exchange model, that $\xi > 3$ for metallic ferromagnetic substances and $\xi < 3$ for ferrimagnetism. Their value of 3.4 may not be too inconsistent with their model of weak ferromagnetism superimposed on antiferromagnetism (canted spins). However, the results of Sec. III-A and Fig. 10 shows that $\xi = 10.8$, which means (M_s/M_o) is a much more rapidly dropping function of (T/T_c) than either 3 or 3.4. This is also seen in the more rapid drop-off of (M_s/M_o) near T_c in Fig. 11 than can be accounted for by a Brillouin curve. On the basis of Vlasov and Vonsovskii's theory, these results would also indicate strong ferromagnetic coupling.

However, the theory of Vlasov and Vonsovskii may not be applicable to MnP and if that is true, other mechanisms may be operating to distort the $M_s(T)$ curve from a Brillouin function. One possibility is the high anisotropy. Callen[45] has shown that the effect of a large anisotropy near the Curie point will be to raise the magnetization over what it would normally be when a field is applied in an easy direction, and to decrease the magnetization in a hard direction. Unfortunately, the mathematical methods break down for the case of uniaxial anisotropy near the Curie point. Another possibility is that temperature dependent exchange interactions will modify the $M_s(T)$ curve. Smart[46] has shown that a modification of the molecular field theory to include competing temperature-dependent interactions will produce exactly this result. The latter mechanism is probably to be preferred over the anisotropy effect since it is consistent with the conclusions reached from the low-temperature results, but both mechanisms could be operating simultaneously.

The measured paramagnetic moment $\mu_{eff} = 2.9$ Bohr magnetons, although significantly lower than Bates'[30] result of 3.69 Bohr magnetons, is nevertheless quite a bit larger than the

spontaneous moment of μ_o = 1.29 Bohr magnetons at T = 0°K, and one must reckon with this in attempting to explain the properties of MnP on the basis of strong ferromagnetic coupling. The magnitude of the discrepancy is revealed by a calculation of the effective angular momentum quantum numbers from the formulas $\mu_o = gJ\beta$ and $\mu_{eff} = g\sqrt{J(J+1)}\beta$. Given g = 2 one obtains J = 0.65 and J = 1.0 from the ferromagnetic and paramagnetic data, respectively. The difference can further be partially attributed to the experimental inaccuracy of ±20 percent in μ_{eff} and the fact that 2.9 Bohr magnetons is actually an upper limit for μ_{eff} since the $1/\chi$ vs T curve may still have some concave curvature even at 200°C. Although one cannot completely rule out the presence of angles between the spins, all the above arguments would imply that any angle or spiraling of the spins in the ferromagnetic state would necessarily be restricted to small cone angles.

The question of why MnP has such a low saturation moment as compared to the ionic value of Mn^{3+} has at least two possible explanations. One approach is to consider spin orbit coupling as Adachi[47] has done in his calculations of the anisotropy in NiAs structures. This interaction has the effect of partially removing any quenching of the orbital momentum with the result that a contribution to the magnetic moment may arise which may couple either parallel or antiparallel to the moment of the spins. However, no specific calculations were done for the MnP structure.

Another approach has been given by Goodenough,[48] who starts with the plausible assumption that the sp electron states are split into a completely full nonmagnetic band and an empty band and that the d states lie in the energy gap. There would be a crystal-field splitting of the d levels that is large enough to put Mn^{3+} in a low-spin state, so that a maximum of J = 1 is anticipated. The further reduction in moment $\mu_o = gJ\beta$ to the measured value of 1.29 Bohr magnetons is attributed to the fact that the Mn-Mn separation is sufficiently small that some of the d electrons are collective. This model also requires that the magnetic moment is a function of temperature due to some of the electrons in a localized state being excited into an overlapping band as the temperature is increased, so that at high temperatures $J \rightarrow 1$ or $\mu_{eff} \rightarrow 2.8\beta$. A further result of this reasoning is that the overlapped band tends to become half full at low temperatures. The latter condition is a requirement for antiferromagnetism in this line of reasoning, and hence the theory would account for a low-temperature antiferromagnetic transformation in a natural way. The dependence of $\mu(T)$ would also account for a distorted Brillouin curve such as has been observed. However, the experimental results cannot distinguish between this model, and the model of competing interactions described in Sec. I and in the next section.

B. Low-Temperature Data

The Weiss molecular field theory of magnetism cannot explain an antiferromagnetic-ferromagnetic transition as has been discussed by Anderson[49] and Pratt.[50] Such transformations have been explained in the rare earths[25,51,52,53] and in MnAs and MnBi[46] on the basis of competing interactions. The metamagnetism and the spiral spin structures in such compounds have also received successful interpretation on this basis. The metamagnetism of MnP makes it a logical candidate for explanation in terms of competing interactions.

The critical field for the onset of ferromagnetism is too low to represent spin flipping in a collinear antiferromagnet, as was discussed in Sec. I. The spin-flip field is on the order of the exchange field ($\approx 10^6$ oe or more) whereas the critical field for MnP ranges from 0 to 2500 oe. Evidence that antiferromagnetic MnP cannot have a simple collinear spin model also comes from the observation of the initial susceptibilities at low temperature. The fact that all the

susceptibilities are the same in the ac plane as $T \rightarrow 0°K$ implies a symmetric structure of spins around the b axis. The normal collinear antiferromagnet would have symmetry about its spin axis, but the susceptibility along the axis would tend to zero at $T = 0°K$. This is not observed in MnP.

The antiferromagnetic spin arrangement of MnP is probably not a simple planar arrangement of spins either such as a triangular arrangement or simple spiral as in Figs. 2(d) and 2(e), respectively. It is expected from calculations of Yoshimori,[25] Enz,[24] and others, that the susceptibility perpendicular to the planes of spins would be greater than any susceptibility within the plane as discussed in Sec. I. In MnP $\chi_b < (\chi_a \text{ or } \chi_c)$ and one would expect the reverse for the above structures.

One model which would account for the observed susceptibilities is a two cone model of spins such as described in Sec. I-A. The umbrella structure of CrSe shown in Fig. 2(f) is such a structure, and it is interesting that CrSe has a NiAs crystal structure with the axis of the observed umbrella spin structure along the crystalline c axis. This crystal axis corresponds to the MnP b axis, which is the low-temperature axis of symmetry in χ.

The transformation at 50°K in MnP is apparently first order, on the basis of a theory due to Smart.[46] Although a discontinuous lattice parameter change probably occurs, there are four important points to be noted:

(1) There is a complete lack of temperature and field hysteresis (< 5 oe and < 0.2°K).

(2) The saturation moment (at 10,000 gauss) is continuous and smooth as a function of temperature through the transition region.

(3) The magnetic symmetry in the ferromagnetic state below 50°K is the same as above 50°K.

(4) The magnetic symmetry in the antiferromagnetic state is also orthorhombic below 50°K, but approaches cylindrical symmetry about the b axis at $T = 4.2°K$.

These facts indicate that there is probably no change in crystal symmetry at 50°K.

Perhaps the most interesting question posed by MnP is why the material should show strong ferromagnetic interactions at high temperature, and yet the presence of competing interactions at low temperatures. The usual antiferromagnetic-ferromagnetic transition is the reverse of this state of affairs: the ferromagnetic state is stabilized at low temperatures. Theories of the spiral structure usually assume that the ferromagnetic state is stabilized at low temperatures due to the temperature dependence of anisotropy. A system of spiraling spins will be stabilized to spiral in an easy plane by the anisotropy, but if there is sufficient anisotropy within the plane, then the increase of anisotropy with decreasing temperature will eventually force the system to reduce its free energy by causing the spins to line up in a ferromagnetic array. However, such cannot be the mechanism in MnP since the antiferromagnetic state is the low-temperature state. One explanation, which is also consistent with the explanation for the distorted $M_s(T)$ curve, is that MnP is subject to competing temperature-dependent magnetic exchange interactions. This mechanism has been given as the cause of the transitions in Dy by Enz[24] and would account for the critical field effect, as discussed in Sec. I. Another possibility is the model proposed by Goodenough, as discussed in Sec. IV-A. A theoretical calculation based on this model may be able to show whether it can also predict the low critical fields for reestablishment of ferromagnetism such as have been observed in MnP.

C. Anisotropy Measurements

One of the most important results of the anisotropy measurements is the regular dependence on temperature of K_1 and K_2. There are no crossover points where one axis becomes easier than another over the entire temperature range. Such a crossover could have provided an alternate explanation for the low-temperature data with its critical field effect, but this is seen not to be the case.

It has been shown, by Akulov,[54] Zener,[55] Van Vleck,[56] Callen,[57] and others, that the temperature dependence of uniaxial anisotropy coefficients ought to be proportional to $(M_s/M_o)^3$, vanishing at the Curie point. It is interesting that MnP has a very large anisotropy which does not vanish at the Curie point as $(M_s/M_o)^3$, but is more like $(M_s/M_o)^2$. This can be seen from Fig. 21. It is shown in Appendix C that an effective field-induced anisotropy can be defined for an anisotropic paramagnetic and that the value of K_p so defined satisfies the relation

$$2K_p/M^2 = 1/\chi_1 - 1/\chi_2 \quad ,$$

where M is the field-induced magnetization and χ_1 and χ_2 are the minimum and maximum values of anisotropy in the plane. It has been shown in Appendix B that the ferromagnetic anisotropy constant K obeys the same relationship and it therefore follows from the results of Table I and Fig. 20 that the ferromagnetic and paramagnetic anisotropies are consistent with each other.

V. CONCLUSIONS

The principal conclusions arrived at in this investigation can now be briefly summarized:

(a) At high temperatures MnP has strong ferromagnetic interactions as evidenced by a concave-upward slope in the $1/\chi$ vs T curve. This eliminates previous speculation that MnP is ferrimagnetic[1] or is antiferromagnetic with weak superimposed ferromagnetism.[2]

(b) A low-temperature transformation (50°K) has been observed which has not been reported previously. At this point MnP becomes metamagnetic, i.e., it exhibits an antiferromagnetic-ferromagnetic transformation which is a function of the direction and magnitude of the external field. This transformation is probably first order but it is not a typical chemical phase change.

The magnetic data indicate that it is extremely likely that the orthorhombic symmetry of the MnP structure is preserved below 50°K. An interpretation of these effects has been made in terms of competing temperature-dependent, magnetic interactions. However, it should be noted that when this theory has been used before it applied to materials which exhibit antiferromagnetism at high temperatures and ferromagnetism at low temperatures. The reverse is true for MnP and a different theory may be needed. An alternate theory proposed by Goodenough[48] has been discussed, but the experimental results are not able to distinguish between the two approaches.

In addition to the above experimental results and conclusions there have been several new technical innovations which, to the author's knowledge, have not been demonstrated before.

First, a simple method of temperature control and temperature cycling has been developed for the vibrating sample magnetometer which involves a thermocouple in direct contact with the sample. This allows control within ±0.04°K at high temperatures, deteriorating somewhat to

±0.2°K at low temperatures. This control is essential to anisotropy measurements in materials where the magnetic properties change rapidly as a function of temperature.

Also, a technique of measuring both the magnitude and the direction of magnetization accurately has been developed (see Appendix C). This is important in anisotropic materials where the magnetization is not always parallel to the applied field. The particular use made of this technique in this investigation was for the measurement of anisotropy in the paramagnetic region. However, it can equally well be applied to ferromagnetic anisotropy measurements.

ACKNOWLEDGMENTS

The author gratefully acknowledges the advice of Professor John T. Norton who supervised this research. He is especially indebted to Dr. John B. Goodenough for his encouragement and for making available the facilities of Group 53 at Lincoln Laboratory. Dr. Dana Ridgley grew the single crystal of MnP and the chemical analysis for Mn content was carried out by Mr. Earl Whipple.

Thanks also go to Mr. Norman Menyuk, Mr. Kirby Dwight, and Dr. Thomas Kaplan for many discussions on the interpretation of the magnetic data.

APPENDIX A
TWO-SUBLATTICE COLLINEAR MODEL

Néel generalized the concept of the Weiss molecular field to two or more sublattices by assuming that interactions of magnetic ions within and between sublattices give rise to distinct internal fields, so that the total Weiss field acting at an atom of the i^{th} sublattice in a υ sublattice system is

$$H_{Wi} = \sum_{j=1}^{\upsilon} W_{ij}M_j \quad , \tag{A-1}$$

where W_{ij} is the internal field constant for the i-j sublattice interaction and M_j is the magnetization in the j^{th} sublattice. For a negative exchange constant $J_{ij} < 0$ (antiparallel coupling between atoms), $W_{ij} < 0$. Also, $W_{ij} = W_{ji}$, since action equals reaction. Now expansion of the Brillouin function for small fields or high temperatures yields the equation

$$M/(H + H_W) = M/(H + WM) = C/T \quad , \tag{A-2}$$

where H_W is the Weiss field. This is the Curie-Weiss law for only one sublattice. However, substitution of Eq. (A-1) into Eq. (A-2) yields

$$M_iT - C_i\left[H + \sum_{j=1}^{\upsilon} W_{ij}M_j\right] = 0 \quad . \tag{A-3}$$

This equation, together with the expression for the total magnetization

$$M = \sum_{j=1}^{\upsilon} M_j \quad , \tag{A-4}$$

can be solved as a pair of simultaneous equations to eliminate the M_i. For the two-sublattice case ($\upsilon = 2$), using the definition for the susceptibility

$$\chi_{mol} \equiv \chi_m \equiv MV_{mol}/H \quad , \tag{A-5}$$

Néel obtained the following expression for χ_m,

$$1/\chi_m = 1/C_m\,[T - \Theta_a - \Theta_b^2/(T - \Theta)] \quad , \tag{A-6}$$

where $C = C_1 + C_2$ and C_1 and C_2 are the Curie constants for the two sublattices as defined by the equation

$$\mu_{eff} = g\sqrt{J(J + 1)}\,\beta = \sqrt{8C_m}\,\beta \quad , \tag{A-7}$$

for each sublattice. Here $g(\approx 2)$ is the gyromagnetic ratio, J the angular momentum, β the Bohr magneton, and C_m is the Curie constant for one mole of material. If there is more than one kind of ion on a given sublattice, a suitable average is generally used.

The paramagnetic temperatures entering Eq. (A-6) are given by

$$\Theta_a = (2C_1C_2W_{12} + C_1^2W_{11} + C_2^2W_{22})\,(C_1 + C_2)^{-1} \quad , \tag{A-8}$$

$$\Theta = (-2W_{12} + W_{11} + W_{22})\,(C_1C_2)\,(C_1 + C_2)^{-1} \quad , \tag{A-9}$$

$$\Theta_b = [(2 - C_1)\,W_{12} + C_1W_{11} - C_2W_{22}]\,C_1C_2\,(C_1 + C_2)^{-1} \quad . \tag{A-10}$$

For an antiferromagnetic material composed of two identical sublattices, $C_1 = C_2$ and $W_{11} = W_{22}$ so that $\Theta_b = 0$. If $\Theta_b = 0$ Eq. (A-6) becomes a Curie-Weiss law with no curvature above $T_c = \Theta_a$. This is the case for antiferromagnetism. For nonequivalent sublattices Eq. (A-6) still asymptotically approaches a Curie-Weiss law at high temperatures with a paramagnetic Curie temperature $\Theta_p = \Theta_a$. It is seen from Eq. (A-8) that Θ_a can be considered as an average of the interactions W_{12}, W_{11}, and W_{22}. Usually, these interactions are considered to be negative for ferrimagnetism (or at least W_{12} is negative and large compared to W_{11} and W_{22}) which means that Θ_a should be negative.

The term involving Θ_b^2 in Eq. (A-6) causes a concave-downward curvature in the $1/\chi_m$ vs T curve. It therefore follows that $\Theta_a < T_c$ even if there are strong competing ferromagnetic interactions.

APPENDIX B
ANISOTROPY MEASUREMENTS AND THE MAGNETIZATION PROCESS

The anisotropy energy $E(\Theta)$ may be defined as the free energy required to rotate a magnetization vector $\vec{M}$ of constant length $|\vec{M}|$ through an angle Θ from some equilibrium or "easy" reference direction by means of an applied field perpendicular to M (see, for instance, Callan[57]). This definition avoids possible changes in energy due to changes $\vec{M} \cdot \vec{H}_i$. Here $\vec{H}_i$ equals the internal field and $\vec{H}_i = \vec{H}_e - n\vec{M}$ for a sphere, where $\vec{H}_e$ is the external field and n is the demagnetizing factor equal to $4\pi/3$. In a sphere this product $\vec{M} \cdot \vec{H}_i$ may change with Θ and $\vec{H}_e$ due to a dependence $\vec{M}(\Theta, H_i)$ near the Curie point. However, at low temperatures $\vec{M}$ can be considered a constant independent of Θ or $\vec{H}_i$ and the usual experimental procedure is to measure the anisotropy in the presence of a large component of $\vec{H}_i$ along $\vec{M}$ so as to remove complicated domain effects.

The anisotropy energy of a material having orthorhombic symmetry has been discussed in the text (see Sec. III-C) and is given by $E = K_1\alpha_2^2 + K_2\alpha_2^2$ where α_1 and α_2 are the direction cosines relative to the a and b axes, the c axis being easy. Since all the measurements to be discussed were made in a principal crystallographic plane with either $\alpha_1 = 0$ (bc plane) or $\alpha_2 = 0$ (ac plane) it follows that either $E = K_1\alpha_1^2 = K_1 \cos^2(90° - \Theta) = K_1 \sin^2\Theta$ for $\alpha_2 = 0$, or $E = K_2 \cos^2(90° - \Theta) = K_2 \sin^2\Theta$ for $\alpha_1 = 0$, where Θ is measured relative to the c axis. This is mathematically equivalent to uniaxial anisotropy and Néel, et al.,[41] have given equations describing the magnetization process in a spherical single crystal having uniaxial anisotropy which describes both the high-field, single domain state and the low-field multidomain state. One can essentially fit these equations to the magnetization data and obtain values for K_1 or K_2. There are three methods which have been used in this report.

(1) At high fields, with a single domain crystal having a magnetization M_s (assumed equal to the spontaneous magnetization) Néel, et al., showed that the following equations apply:

$$\sin 2\Theta = (H_e M_s/K) \sin(\varphi - \Theta) \qquad \text{(B-1a)}$$

$$M_H = M_s \cos(\varphi - \Theta) \quad , \qquad \text{(B-1b)}$$

where K is either K_1 or K_2 depending on the plane, φ is the angle between the external field and the c axis and M_H is the component of M_s along the field (measuring) direction. These equations can be solved simultaneously to eliminate the unknown angle Θ. This was done in the bc plane for a variety of conditions such as H_e constant, φ and M variable, or M constant, φ and H_e variable. The vibrating sample magnetometer is easily adapted to this kind of measurement, since the reference signal can be preset to a particular value of M_H, for instance, and then H_e and φ varied so as to give a series of different null points. A particularly simple expression obtains if we require that $M_H/M_s = \sqrt{1/2} = 0.707$. Simultaneous solution of Eq. (B-1a) and Eq. (B-1b) yields

$$\cos 2\varphi = -(H_e M_s/\sqrt{2}K) \quad . \qquad \text{(B-2)}$$

If we plot H_e vs $(-\cos 2\varphi)$ a straight line should be obtained with a slope of $(\sqrt{2}K/M_s)$. Since M_s is known from measurement, the value of K can be obtained. This was done for two quadrants of φ in the bc plane and the results at T = 77°K are shown in Fig. B-1. It was found by this method that $(2K_2/M_s^2) = 40.4$ at 77°K. The fact that the two lines of Fig. B-1 do not fall on

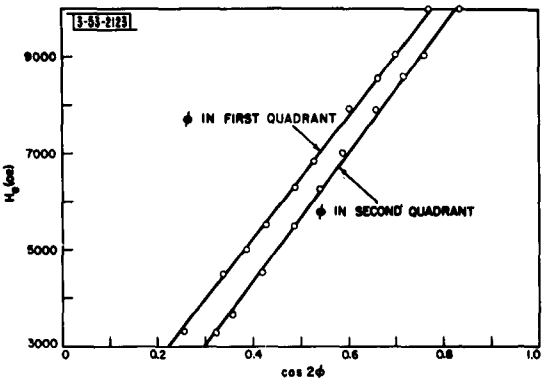

Fig. B-1. H_e vs cos 2ϕ. Test of the Néel model.

top of each other is due to the c axis not coinciding exactly with $\varphi = 0$. However, this error makes little difference in the slope.

(2) Even though the multidomain, low-field case is more complicated than the single domain case, the situation is not too bad for uniaxial anisotropy. Néel, et al., have shown that at low fields the initial portion of the magnetization curves is linear with field and they derive an effective susceptibility

$$\chi \equiv M_H/H_e = (M + N \cos^2 \varphi)/n(n + N) \quad , \tag{B-3}$$

where M_H is the measured component of the net measured magnetization (not M_s) along the field direction. H_e is the external field, n is the demagnetizing constant = $4\pi/3$ and $N = 2K/M_s^2$ where K would be K_1 for the ac plane or K_2 for the bc plane. If N is not too large, a plot of χ vs $\cos^2 \varphi$ provides a test of the Néel model since a straight line should be obtained with a slope of $N/n(n + N)$. For large N this slope approaches $1/n$ and the slope is insensitive to the effect of anisotropy. The plot of χ vs $\cos^2 \varphi$ in Fig. 20 is a straight line and gives a value for $N = 2K_2/M_s^2 = 40.2$ for the bc plane at 77°K which is in good agreement with Method (1). A similar plot was made for the ac plane, but it was much more difficult to determine the value of K_1 with any certainty, because of the much larger value of $N = 2K_1/M_s^2$.

(3) The easiest way to determine the anisotropy is simply from measurement of the effective susceptibility along the three orthorhombic axes. However, this measurement is only good as a first-order indication of the anisotropy and cannot be made reliably until one has at least established that the domains are not "frozen" in some metastable equilibrium direction. This possibility was checked by cooling the sample through the Curie point to the lowest temperatures to be investigated in the presence of a 10,000-gauss "annealing" field. No irreversible effects were found, provided the sample was securely cemented, and all results were the same as for no annealing field.

The Néel equations above yield

$$1/\chi_c = n \quad , \quad 1/\chi_a = n + 2K_1/M_s^2 \quad , \quad 1/\chi_b = n + 2K_2/M_s^2 \quad , \tag{B-4}$$

where χ_a, χ_b, and χ_c are the effective susceptibilities along the a, b, and c axes. These equations lead to

$$1/\chi_a - 1/\chi_c = 2K_1/M_s^2 \quad , \quad 1/\chi_b - 1/\chi_c = 2K_2/M_s \quad , \tag{B-5}$$

so that K_1 and K_2 can be determined simply from χ_a, χ_b, and χ_c. The value for $2K_2/M_s^2$ determined in this way for the bc plane at 77°K was 39.7, which is in excellent agreement with the other two methods discussed. Since annealing experiments showed no complicating effects, and since such good agreement was obtained between the three methods for K_1, the rest of the anisotropy measurements were performed by this last method.

Finally, it is pointed out that the difference between the two values of $(1/\chi)$ (for two different temperatures, or two different directions in the crystal) need not be corrected for the demagnetizing factor. This follows directly from the definition of the effective susceptibility $\chi \equiv M_H/H_e$, where H_e is the external field. Therefore, the true susceptibility χ_T is given by

$$1/\chi_T \equiv H_i/M_H = (H_e - nM_H)/M_H = (H_e/M_H) - n = (1/\chi) - n \quad , \qquad \text{(B-6)}$$

where H_i is the component of internal field along the measuring direction. It is seen that the demagnetizing factor n drops out if the difference is taken between two values of $1/\chi$. This is further seen in the disappearance of n from Eq. (B-5).

APPENDIX C
PARAMAGNETIC ANISOTROPY

The susceptibility in an anisotropic crystal is a tensor rather than a scalar, but simple relations can be used to derive the equations pertinent to this investigation. Let us assume that we have a paramagnetic material which can be characterized by principal susceptibilities χ_a, χ_b, and χ_c, along the three orthorhombic a, b, and c axes, such that the magnetization $\vec{M}$ along an arbitrary direction is given by

$$\vec{M} = \chi_a H_a \vec{V}_a + \chi_b H_b \vec{V}_b + \chi_c H_c \vec{V}_c \quad , \tag{C-1}$$

where H_a, H_b, and H_c are the a, b, and c axis components of the internal field and $\vec{V}_a$, $\vec{V}_b$, and $\vec{V}_c$ are unit vectors along the axes.

In such a material the magnetization will not be in the direction of the applied field and it is a difficult thing to determine if the material satisfies the above conditions. This was done for the bc plane in MnP by constructing a set of pickup coils which could be rotated about an axis passing through the sample parallel to the drive rod of the magnetometer. The magnitude of M could thus be measured to ±1 percent even if its direction did not coincide with $\vec{H}_e$ (the external field) by simply rotating the coils until a maximum signal was recorded. ($\vec{M}$ was assumed to lie in the bc plane with an applied field in this plane. There was no reason to think otherwise since the three magnetic symmetry axes coincided with the three crystallographic axes a, b, and c and since the relative magnetic hardness of the three axes a > b > c was preserved throughout the ferromagnetic and paramagnetic regions. Further support for this came from direct observation of the fact that $\vec{M}$ stayed in the bc plane with a field applied in this plane in the ferromagnetic state. The latter measurement was also accomplished through the use of the rotating coil holder.)

The rotating coil holder also permitted locating the direction of $\vec{M}$ to better than 1° by rotating the pickup coils until a null was detected, the axis of the coils then being perpendicular to $\vec{M}$. By thus locating both the direction and magnitude of $\vec{M}$ it was possible to show that Eq. (C-1) was satisfied.

Given the above description of magnetic properties, let us ask what the paramagnetic anisotropy is. Consistent with the definition of anisotropy in Appendix B, let us ask how much energy is required to rotate a constant vector $|\vec{M}|$ away from the direction c (assuming $\chi_c < \chi_b$) by an angle Θ. (This should also be consistent with the definition of ferromagnetic anisotropy.) Since the magnetic energy $E = 1/2\ \vec{M} \cdot \vec{H}$, we have

$$E = 1/2\ M_b H_b + 1/2\ M_c H_c \quad , \tag{C-2}$$

where M_b, M_c are the b and c axis components of $\vec{M}$, and H_b and H_c are the b and c axis components of the internal field. Now, since $M_b = \chi_b H_b$ and $M_c = \chi_c H_c$, we have

$$E = 1/2\ (M_b^2/\chi_b + M_c^2/\chi_c) \quad , \tag{C-3}$$

and since $M_b = M \sin\Theta$, $M_c = M \cos\Theta$,

$$E = 1/2\ M^2 \sin^2\Theta/\chi_b + 1/2\ M^2 \cos^2\Theta/\chi_c$$

$$= 1/2\ M^2 \sin^2\Theta\ (1/\chi_b - 1/\chi_c) + 1/2\ M^2/\chi_c \quad . \tag{C-4}$$

Since $M^2/2\chi_c$ is a constant term, Eq. (C-4) can be compared to the case of ferromagnetic uniaxial anisotropy $E = K_2 \sin^2 \Theta$ (for the bc plane) if

$$2K_{P2}/M^2 = 1/\chi_b - 1/\chi_c \quad , \tag{C-5}$$

where we have defined a paramagnetic anisotropy constant K_{P2} which should be equivalent to K_2 for ferromagnetism. It is seen that Eq. (C-5) is exactly Eq. (B-5) for ferromagnetic anisotropy in the bc plane if M is replaced by M_s. Therefore, measuring χ_b and χ_c and computing $1/\chi_b - 1/\chi_c$ should give the paramagnetic anisotropy consistent with the ferromagnetic anisotropy. A similar procedure can be carried out for the ac plane yielding

$$2K_{P1}/M^2 = 1/\chi_a - 1/\chi_c \quad . \tag{C-6}$$

This argument shows that the values of Table I give $2K_{P1}/M^2$ in the paramagnetic region, which should go smoothly over into $2K_1/M_s^2$ in the ferromagnetic region, and it shows the validity of comparing Table I to the plot of $2K_1/M_s^2$ in Fig. 21.

REFERENCES

1. Ch. Guillaud, Compt. rend. 235, 468 (1952).
2. V.P. Krasovskii and I.G. Fakidov, Fiz. Metal. i Metalloved. 11, No.2, 319-320 (1961).
3. P. Weiss, J. Phys. 6, 661 (1907).
4. W. Heisenberg, Z. Physik 49, 619 (1928).
5. E.C. Stoner, Proc. Leeds Phil. Mag. 3, 457 (1937).
6. K.P. Belov, Magnetic Transitions (Consultants Bureau, New York, 1959) p. 25.
7. E.C. Stoner, Proc. Roy. Soc. (London) 165A, 372 (1938).
8. L. Néel, Ann. phys. 3, 137-198 (1948).
9. T. Nagamiya, K. Yosida and R. Kubo, Adv. Phys. 4, No. 13 (1955).
10. S. Foner and S. Hon, J. Appl. Phys. 33S, 1289 (1962).
11. T. Moriya, Phys. Rev. 120, 91 (1960).
12. I. Dzyaloshinsky, J. Phys. Chem. Solids 4, 241 (1958).
13. Y. Yafet and C. Kittel, Phys. Rev. 87, 290 (1952).
14. J. M. Luttinger, Phys. Rev. 119, 1153 (1960).
15. T. A. Kaplan, K. Dwight, D. H. Lyons and N. Menyuk, J. Appl. Phys. 32S, 13 (1961).
16. D. Lyons and T. A. Kaplan, Phys. Rev. 120, 1580 (1960).
17. L. M. Corliss, N. Elliott, J. M. Hastings and R. L. Sass, Phys. Rev. 122, 290 (1952).
18. D. R. Behrendt, S. Legvold and F. H. Spedding, Phys. Rev. 109, 1544 (1958).
19. B. D. Rhodes, S. Legvold and F. H. Spedding, Phys. Rev. 109, 1547 (1958).
20. J. F. Elliott, S. Legvold and F. H. Spedding, Phys. Rev. 100, 1595 (1955).
21. R. W. Green, S. Legvold and F. H. Spedding, Phys. Rev. 122, 122 (1961).
22. M. K. Wilkinson, W. C. Koehler, E. O. Wollan and J. W. Cable, J. Appl. Phys. 32, 48S (1961).

23. W. C. Koehler and M. K. Wilkinson, J. Appl. Phys. 32, 48S (March 1961).
24. U. Enz, J. Appl. Phys. 32, 22S (March 1961).
25. A. Yoshimori, J. Phys. Soc. Japan 14, 807 (1959).
26. T. A. Kaplan, Phys. Rev. 124, 329 (1961).
27. H. Nowotny, Z. Electrochem. 49, 254 (1943).
28. H. Nowotny, Z. Physik. Chem. Abt. B 38, 356 (1937).
29. K. H. Sweeny and A. B. Scott, J. Chem. Phys. 22, No. 5, 917 (1954).
30. L. F. Bates, Phil. Mag. 8, 714 (1929).
31. B. G. Whitmore, Phil. Mag. 7, 125 (1929).
32. Ch. Guillaud and H. Creveaux, Compt. rend. 224, 266 (1947).
33. Ch. Guillaud, Compt. rend. 235, 468 (1952).
34. I. G. Fakidov and V. P. Krasovskii, Soviet Phys.-JETP 36, No. 4, 755 (1959).
35. S. V. Vonsovskii and K. B. Vlasov, J. Exptl. Theoret. Phys. (USSR) 25, 327 (1953).
36. S. Foner, Rev. Sci. Instr. 30, No.7, 548 (1959).
37. D.E. Martz, Rev. Sci. Instr. 33, No.2, 214 (1961).
38. P. Weiss and R. Forrer, Ann. Phys. [10] 5, 153 (1926).
39. L. F. Bates, Modern Magnetism (Cambridge University Press, England, 1951).
40. D. O. Smith, Phys. Rev. 102, 959 (1956).
41. L. Néel, R. Pauthenet, G. Rinet and V. X. Giron, J. Appl. Phys. 31, 27S (1960).
42. R. M. Bozorth, Ferromagnetism (D. Van Nostrand, New Jersey, 1956) [see also Equation (2)].
43. C. Kittel, Solid State Physics (Wiley, New York, 1957).
44. S. V. Vonsovskii and K. B. Vlasov, J. Exptl. Theoret. Phys. (USSR) 25, 327 (1953).
45. E. R. Callen and H. B. Callen, J. Phys. Chem. Solids 16, 310 (1960).
46. J. S. Smart, Phys. Rev. 90, 55 (1953).
47. K. Adachi, J. Phys. Soc. Japan 16, 2187 (1961).
48. J. B. Goodenough (private communication).
49. P. W. Anderson, Phys. Rev. 79, 705 (1950).
50. G. W. Pratt, Phys. Rev. 108, 1233 (1957); J. Appl. Phys. 29, 520 (1958).
51. T. Nagamiya, J. phys. radium 20, 70 (1959).
52. J. Villain, J. Phys. Chem. Solids 11, 303 (1959).
53. T. A. Kaplan, Phys. Rev. 116, 888 (1959).
54. N. Akulov, Z. Physik 100, 197 (1936).
55. C. Zener, Phys. Rev. 96, 1335 (1954).
56. J. H. Van Vleck, Grenoble Conference on Magnetism [see J. phys. radium 20 (1959)].
57. E. R. Callen, J. Appl. Phys. 33, 832 (1962).